

Chiral 2D p -wave superfluid from s -wave pairing in the BEC limit

K. Thompson,¹ J. Brand,² and U. Zülicke^{1,3,*}

¹*Dodd-Walls Centre for Photonic and Quantum Technologies, School of Chemical and Physical Sciences, Victoria University of Wellington, PO Box 600, Wellington 6140, New Zealand*

²*Dodd-Walls Centre for Photonic and Quantum Technologies, Centre for Theoretical Chemistry and Physics, and New Zealand Institute for Advanced Study, Massey University, Private Bag 102904 NSMC, Auckland 0745, New Zealand*

³*Department of Physics, University of Basel, Klingelbergstrasse 82, CH-4056 Basel, Switzerland*
(Dated: May 12, 2022)

Two-dimensional spin-orbit-coupled Fermi gases subject to s -wave pairing can be driven into a topological phase by increasing the Zeeman spin splitting beyond a critical value. In the topological regime, the system exhibits the hallmarks of chiral p -wave superfluidity, including exotic Majorana excitations. Previous theoretical studies of this realization of a two-dimensional topological Fermi superfluid have focused on the BCS limit where the s -wave Cooper pairs are only weakly bound and, hence, the induced chiral p -wave order parameter has a small magnitude. Motivated by the goal to identify potential new ways for the experimental realization of robust topological superfluids in ultra-cold atom gases, we study the BCS-to-BEC crossover driven by increasing the Cooper-pair binding energy for this system. In particular, we obtain phase diagrams in the parameter space of two-particle bound-state energy and Zeeman spin-splitting energy. Ordinary characteristics of the BEC limit, in particular the shrinking and eventual disappearance of the Fermi surface, are observed in the nontopological regime. In contrast, the topological phase retains all features of chiral p -wave superfluidity, including a well-defined underlying Fermi surface, even in the limit of large s -wave pair-binding energies. Compared to the BCS limit, the topological superfluid in the BEC limit turns out to be better realizable even for only moderate magnitude of spin-orbit coupling because the chiral p -wave order parameter is generally larger and remnants of s -wave pairing are suppressed. We identify optimal parameter ranges that can aid further experimental investigations and elucidate the underlying physical reason for the persistence of the chiral p -wave superfluid.

I. INTRODUCTION AND OVERVIEW OF MAIN RESULTS

One of the earliest proposed pathways towards realization of a two-dimensional (2D) topological superfluid (TSF) [1] is based on s -wave pairing of 2D fermions subject to spin-orbit coupling and Zeeman spin splitting [2–6]. When the Zeeman energy h exceeds the critical value

$$h_c = \sqrt{\mu^2 + |\Delta|^2} \quad , \quad (1)$$

with Δ and μ denoting the s -wave pair potential and chemical potential, respectively, the system's low-energy sector [7] mirrors the properties of a chiral 2D p -wave superfluid [8]. In particular, exotic Majorana excitations are present at boundaries [2, 9] and in vortex cores [10–14] that could be utilized for fault-tolerant quantum-information processing [15]. Intense efforts towards experimental implementation of 2D TSFs using the above-described route have so far been thwarted by the deleterious effect of Zeeman-splitting-inducing magnetic fields on superconductivity in typical materials [16], as well as basic physical constraints on the magnitude of spin-orbit coupling reachable in solids [17] and ultra-cold atom gases [18, 19]. Our present study shows that a possible way around the latter limitation would be to access the

strong-coupling regime of the s -wave pairing, which is commonly referred to as the BEC limit [20–24].

The main insights reached in our work are underpinned by zero-temperature mean-field phase diagrams [25] in the parameter space of two-particle s -wave bound-state energy E_b and Zeeman energy h as illustrated in Fig. 1. These feature a first-order phase-transition region that truncates the second-order topological-transition line $h_c(E_b)$. In this region, the system cannot assume a single-phase equilibrium ground state but instead phase-separates into domains of different densities. Critical Zeeman-energy values $h_<$ and $h_>$ delimit the phase-separation region at fixed E_b , defining two curves in the phase diagram that merge at a critical end point $(h^{(c)}, E_b^{(c)})$ defined by the condition

$$h^{(c)} \equiv h_<(E_b) \Big|_{E_b=E_b^{(c)}} \stackrel{!}{=} h_>(E_b) \Big|_{E_b=E_b^{(c)}} \quad . \quad (2)$$

The properties of the phase-separation region itself have been the subject of previous work [26, 27], and we also provide a few more details later on. However, the main focus of our present study is the careful determination of the location of the boundaries $h_<$ and $h_>$ and the exploration of the adjacent homogeneous phases, especially in the limit of large E_b/E_F .

Comparison of our results with those obtained previously for spin-imbalanced 2D Fermi superfluids [28] helps to elucidate the physical consequences of finite spin-orbit coupling. The magnitude of the latter is most conveniently measured in terms of the dimensionless parameter

* uli.zuelicke@vuw.ac.nz

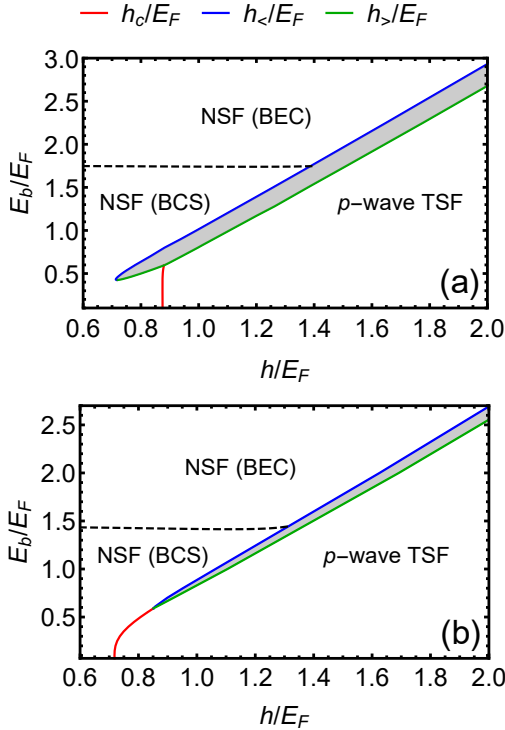


FIG. 1. Zero-temperature mean-field phase diagrams, in the parameter space of two-particle s -wave bound-state energy E_b and Zeeman energy h , for a spin-orbit-coupled 2D Fermi gas with fixed density $n = mE_F/(\pi\hbar^2) \equiv k_F^2/(2\pi)$. Panel (a) [(b)] depicts the case where the dimensionless parameter $\lambda k_F/E_F$ measuring the spin-orbit-coupling strength equals 0.50 [0.75], which is in the small-(large)-spin-orbit-coupling regime. The shaded region $h_< < h < h_>$, with $h_<$ ($h_>$) indicated by the blue (green) line, is in the phase-separated first-order-transition regime that emerges for $E_b > E_b^{(c)}$ and $h > h^{(c)}$. The critical Zeeman energy h_c , defined via Eq. (1) and indicated by the red curve, delineates the second-order transition between an ordinary nontopological superfluid (NSF) and a topological superfluid (TSF). From the point when the $h_c(E_b)$ -curve reaches the region where phase separation occurs, the topological transition is switched from second to first order. The BCS-to-BEC-crossover boundary (dashed line) has been determined via the condition $\mu(E_b, h) = 0$.

$\lambda k_F/E_F$ that also involves the density-dependent Fermi energy $E_F \equiv \hbar^2 k_F^2/(2m)$. One important effect of finite λ turns out to be that the critical end point of the phase-separation region is shifted from its $\lambda = 0$ location [29] at $h^{(c)} = 0$ and $E_b^{(c)} = 0$ to a point with $h^{(c)} > 0$ and $E_b^{(c)} > 0$. The second major impact of finite spin-orbit coupling is the existence of a 2D TSF phase [27] for sufficiently high Zeeman energy $h > \max\{h_c, h_>\}$ in place of the fully polarized normal phase found for $\lambda = 0$ [29].

Our present study shows that the character of the TSF phase emerging in the BEC regime of the underpinning s -wave pairing ($E_b/E_F \gtrsim 1$) is fundamentally no different from the TSF occurring in the BCS limit ($E_b/E_F \ll 1$). In particular, for the entire TSF region in the phase dia-

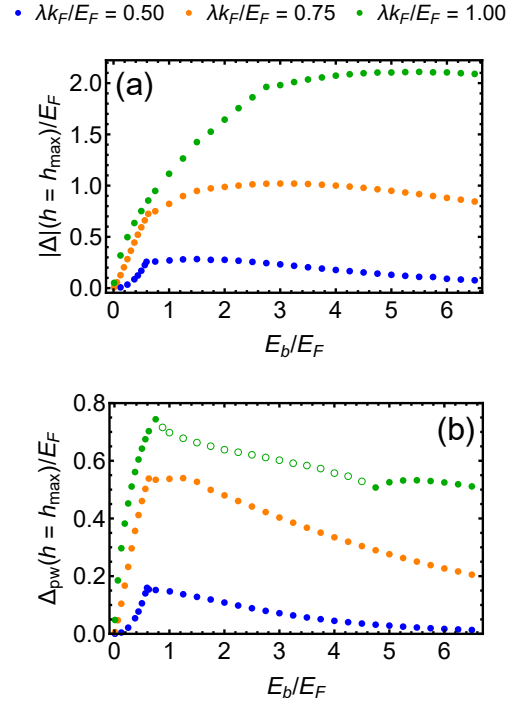


FIG. 2. The magnitude of the s -wave pair potential Δ in the homogeneous topological-superfluid phase of a spin-orbit-coupled 2D Fermi gas with fixed density $n = mE_F/(\pi\hbar^2) \equiv k_F^2/(2\pi)$ is maximized, for fixed two-particle bound-state energy E_b and spin-orbit-coupling strength λ , right after the transition at Zeeman energy $h_{\max} = \max\{h_c, h_>\}$ (cf. Fig. 1). Panel (a) shows the dependence of this maximum value, $|\Delta|_{h=h_{\max}}$, on E_b for three fixed values of λ . Panel (b) is a plot of the emergent chiral- p -wave gap Δ_{pw} , extracted from the low-energy quasiparticle dispersion, for the same parameters. Open symbols indicate data points for the case $\lambda k_F/E_F = 1$ that were obtained for a slightly higher $h = h_{\max} + \delta h$, with $\delta h/h_{\max} < 7\%$, to avoid distortions appearing in the dispersions right after the transition for large spin-orbit coupling.

gram, both the quasiparticle dispersion and the single-particle occupation-number distribution in momentum space exhibit all signatures for the presence of an underlying Fermi surface [30]. This is in stark contrast to the nontopological superfluid (NSF) phase where, deep in the BEC regime, any remnants of a Fermi surface have disappeared as expected from the known phenomenology of the BCS-to-BEC crossover for s -wave pairing [31–33] and illustrated by recent Quantum-Monte-Carlo results obtained for $h = 0$ [34]. Detailed evidence for the unexpectedly universal BCS-regime characteristic of the TSF is provided further below. Among its physical implications is the tantalizing opportunity to explore the canonical properties of topological chiral p -wave superfluidity in this system even in the regime of strong s -wave pairing.

The defining element of the 2D TSF is an emergent chiral p -wave order parameter whose magnitude is proportional to the spin-orbit-coupling strength λ , the modulus $|\Delta|$ of the s -wave pair potential, and the inverse of the

Zeeman energy [3, 5–7, 35]. Given that increasing λ has adverse side effects such as heating of the atom gas [18] in currently available experimental schemes, maximizing the chiral p -wave order parameter needs to be pursued by other means. As $|\Delta|/E_F$ is a monotonously increasing function of E_b/E_F but is suppressed with increasing h/E_F (see, e.g., Refs. [7, 36] and below), its practically largest magnitude occurs just after the transition to the homogeneous TSF phase at $h_{\max} = \max\{h_c, h_\>\}$. Figure 2(a) illustrates the dependence of this value, $|\Delta|_{h=h_{\max}}$, on both E_b and λ . It reveals a maximum that gets broader and larger as the parameter $\lambda k_F/E_F$ increases. As the maximum value of $|\Delta|$ reaches values up to $\sim E_F$ typically, even for only moderately high values of the spin-orbit-coupling strength, the TSF realized in the BEC limit of s -wave pairing presents a much more robust platform for useful study and application than would be available in the BCS regime at the same value of λ . This is established even more directly from considering the gap Δ_{pw} in the low-energy quasiparticle dispersion for the TSF that constitutes a measure for the chiral p -wave order parameter. The values for Δ_{pw} arising for the same parameter combinations that maximize $|\Delta|$ are shown in Fig. 2(b). For all three fixed values of $\lambda k_F/E_F$, a maximum of Δ_{pw} occurs for $E_b/E_F \sim 1$, followed by a broad range for which Δ_{pw} is only slowly decreasing. In regimes of large spin-orbit coupling $\lambda \gtrsim h_{\max}/k_F$, dispersion curves are distorted and Δ_{pw} can be obscured right after the transition, but the latter always emerges clearly at higher Zeeman energies.

The remainder of this article is organized as follows. Section II introduces the theoretical approach used by us to describe the BCS-to-BEC crossover for the s -wave-

paired 2D Fermi gas subject to both spin-orbit coupling and Zeeman spin splitting. Detailed results obtained within this formalism for the system with fixed uniform particle density are presented in the subsequent Sec. III, together with a discussion of physical implications. Our conclusions are formulated in the final Sec. IV.

II. MICROSCOPIC MODEL OF THE 2D TSF

We utilize a standard Bogoliubov-de Gennes (BdG) mean-field formalism [37] to calculate the quasiparticle spectrum for our system of interest. All relevant thermodynamic quantities can be expressed in terms of the obtained eigenenergies and eigenstates. Throughout this work, we consider the zero-temperature limit.

The BdG Hamiltonian of the 2D spin-orbit coupled Fermi gas with s -wave interactions and Zeeman spin splitting $2h$ acting in the four-dimensional Nambu space of spin-1/2 fermions is [38]

$$\mathcal{H} = \begin{pmatrix} \epsilon_{\mathbf{k}\uparrow} - \mu & \lambda_{\mathbf{k}} & 0 & -\Delta \\ \lambda_{\mathbf{k}}^* & \epsilon_{\mathbf{k}\downarrow} - \mu & \Delta & 0 \\ 0 & \Delta^* & -\epsilon_{\mathbf{k}\uparrow} + \mu & \lambda_{\mathbf{k}}^* \\ -\Delta^* & 0 & \lambda_{\mathbf{k}} & -\epsilon_{\mathbf{k}\downarrow} + \mu \end{pmatrix}, \quad (3)$$

where $\epsilon_{\mathbf{k}\uparrow(\downarrow)} = \epsilon_{\mathbf{k}} (\mp) h$ with $\epsilon_{\mathbf{k}} = \hbar^2(k_x^2 + k_y^2)/2m$, and $\lambda_{\mathbf{k}}$ is the spin-orbit coupling [39]. The BdG equation reads

$$\mathcal{H} \begin{pmatrix} u^\uparrow \\ u^\downarrow \\ v^\uparrow \\ v^\downarrow \end{pmatrix} = E \begin{pmatrix} u^\uparrow \\ u^\downarrow \\ v^\uparrow \\ v^\downarrow \end{pmatrix}. \quad (4)$$

Its spectrum consists of four eigenvalue branches [26, 40],

$$E_{\mathbf{k}\alpha, <(>)} = \alpha \sqrt{(\epsilon_{\mathbf{k}} - \mu)^2 + |\Delta|^2 + h^2 + |\lambda_{\mathbf{k}}|^2 (\mp) 2 \sqrt{(\epsilon_{\mathbf{k}} - \mu)^2 (h^2 + |\lambda_{\mathbf{k}}|^2) + |\Delta|^2 h^2}}, \quad (5)$$

with associated eigenspinors $(u_{\mathbf{k}\alpha, \eta}^\uparrow, u_{\mathbf{k}\alpha, \eta}^\downarrow, v_{\mathbf{k}\alpha, \eta}^\uparrow, v_{\mathbf{k}\alpha, \eta}^\downarrow)^T$, where $\alpha \in \{+, -\}$ and $\eta \in \{<, >\}$ label the four different energy-dispersion branches.

The chemical potential μ and magnitude $|\Delta|$ of the pair potential need to be determined self-consistently from solutions of the BdG equations in conjunction with the gap equation and the constraint that the uniform particle density is fixed at $n \equiv k_F^2/(2\pi)$. Corresponding conditions can be formulated mathematically in terms of the energy spectrum and BdG-Hamiltonian eigenspinor amplitudes. See, e.g., Refs. [7, 37]. However, educated by the insights gained from previous work on spin-imbalanced Fermi superfluids [41], we base self-consistency considerations on the properties of the system's grand-canonical ground-state energy density [26,

40, 42, 43], for which a standard calculation yields

$$\mathcal{E}_{\text{gs}}^{(\text{MF})}(|\Delta|, \mu) = \frac{1}{A} \sum_{\mathbf{k}} \left(\frac{|\Delta|^2}{2\epsilon_{\mathbf{k}} + E_b} + \epsilon_{\mathbf{k}} - \mu - \frac{1}{2} \sum_{\eta} E_{\mathbf{k}+, \eta} \right). \quad (6)$$

Here A denotes the system's volume (area), and $E_b > 0$ is the magnitude of the two-particle bound-state (i.e., binding) energy in the absence of spin-orbit coupling [18]. The gap and number-density equations can be expressed in terms of derivatives of the ground-state energy density;

$$\frac{\partial \mathcal{E}_{\text{gs}}^{(\text{MF})}}{\partial |\Delta|} = 0, \quad (7a)$$

$$\frac{\partial \mathcal{E}_{\text{gs}}^{(\text{MF})}}{\partial \mu} = -n. \quad (7b)$$

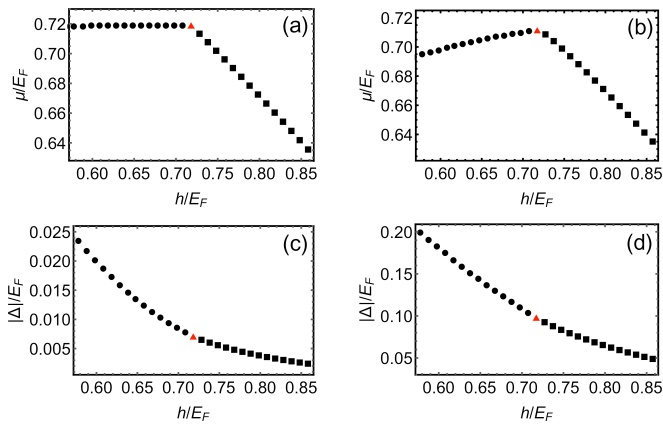


FIG. 3. Chemical potential μ and magnitude $|\Delta|$ of the s -wave pair potential for a spin-orbit-coupled 2D Fermi system with fixed density $n = mE_F/(\pi\hbar^2) \equiv k_F^2/(2\pi)$ in the BCS limit for s -wave pairing, plotted as a function of Zeeman splitting h . Results shown are obtained as solutions of the self-consistency conditions [Eqs. (7a) and (7b)] for $\lambda k_F/E_F = 0.75$ (all panels) and $E_b/E_F = 0.010$ [panels (a) and (c)], 0.10 [panels (b) and (d)]. Data points indicated by circles (a triangle, squares) correspond to states where the system is nontopological (critical, topological), i.e., $h < (=, >) \sqrt{\mu^2 + |\Delta|^2}$.

The lengthy explicit expressions are omitted here.

As emphasized previously during the study of spin-imbalanced Fermi superfluids [44], proper application of the condition (7a) for identifying physical ground states requires ensuring that $\mathcal{E}_{\text{gs}}^{(\text{MF})}(|\Delta|, \mu)$, taken as a function of $|\Delta|$ at fixed μ , has a global minimum at the self-consistently determined value for $|\Delta|$. However, identifying local minima as well as maxima of the ground-state energy at fixed μ can also be of interest [45–47], e.g., to discuss nonequilibrium-dynamic phenomena; hence, we will track these in the following also.

The relative magnitude of E_b with respect to the Fermi energy $E_F \equiv \hbar^2 k_F^2/(2m) = \pi\hbar^2 n/m$ drives the BCS-to-BEC crossover for s -wave pairing in our system of interest [22]. More specifically, we have

$$\frac{E_b}{E_F} \begin{cases} \ll 1 & \text{in the BCS limit,} \\ \gtrsim 1 & \text{in the BEC limit.} \end{cases} \quad (8)$$

In the following, we absorb any dependence on total particle density n by measuring all energies and wave vectors in units of E_F and k_F , respectively. Thus the set of externally tuneable parameters comprises E_b/E_F , h/E_F , and $\lambda k_F/E_F$, where $\lambda \equiv |\lambda_{\mathbf{k}}|/k$. The system's state is characterized by $|\Delta|/E_F$ and μ/E_F .

III. RESULTS AND DISCUSSION

To ground ourselves in well-known results [7, 36], we start by fixing a value for $\lambda k_F/E_F$ and consider the variation of the chemical potential μ and the pair-potential

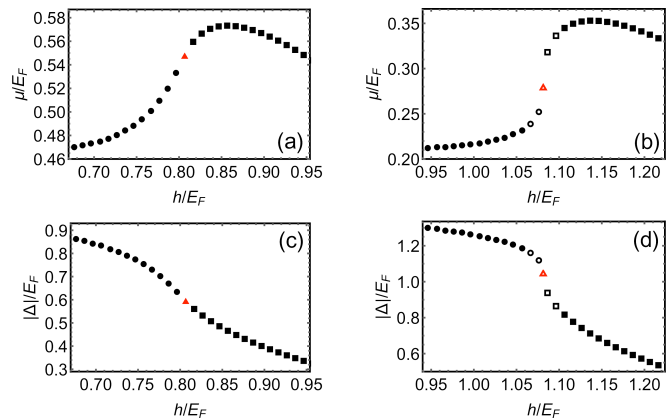


FIG. 4. Chemical potential μ and s -wave pair-potential magnitude $|\Delta|$ for a spin-orbit-coupled 2D Fermi system with fixed density close to the BEC limit for s -wave pairing. Results shown are obtained as solutions of the self-consistency conditions for $\lambda k_F/E_F = 0.75$ (all panels) and $E_b/E_F = 0.50$ [panels (a) and (c)], 1.0 [panels (b) and (d)]. Circles (a triangle, squares) correspond to states where the system is nontopological (critical, topological). Filled (empty) symbols indicate solutions of the self-consistency conditions that globally minimize the ground-state energy and thus correspond to proper equilibrium states of the system (that represent only a local minimum or even a maximum of the ground-state energy).

magnitude $|\Delta|$ as a function of the Zeeman energy h in the BCS limit for s -wave pairing, i.e., for small E_b/E_F . As illustrated in Fig. 3, both $\mu(h)$ and $|\Delta(h)|$ evolve continuously from the nontopological regime where $h < h_c$ [cf. Eq. (1)] via their critical values $\mu_c \equiv \mu(h_c)$ and $|\Delta(h_c)| \equiv \Delta_c$ that satisfy $\sqrt{\mu_c^2 + \Delta_c^2} = h_c$ into the topological phase where $h > h_c$. This reflects the fact that,

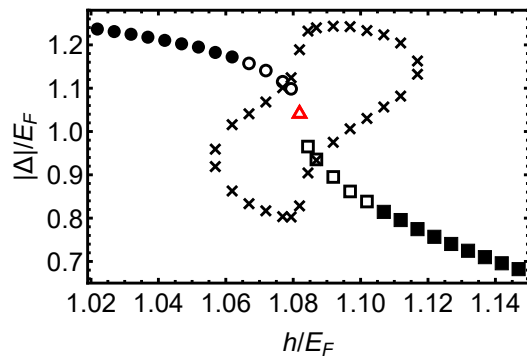


FIG. 5. Emergence of additional zeros of the gap equation close to the BEC limit. Results shown are obtained for $\lambda k_F/E_F = 0.75$ and $E_b/E_F = 1.0$. Filled symbols indicate solutions of the self-consistency conditions that globally minimize the ground-state energy and thus correspond to proper equilibrium states of the system. Empty symbols (crosses) are associated with (non-)self-consistent values corresponding to a local minimum or maximum of the ground-state energy. Circles (a triangle, squares) indicate self-consistent solutions where the system is nontopological (critical, topological).

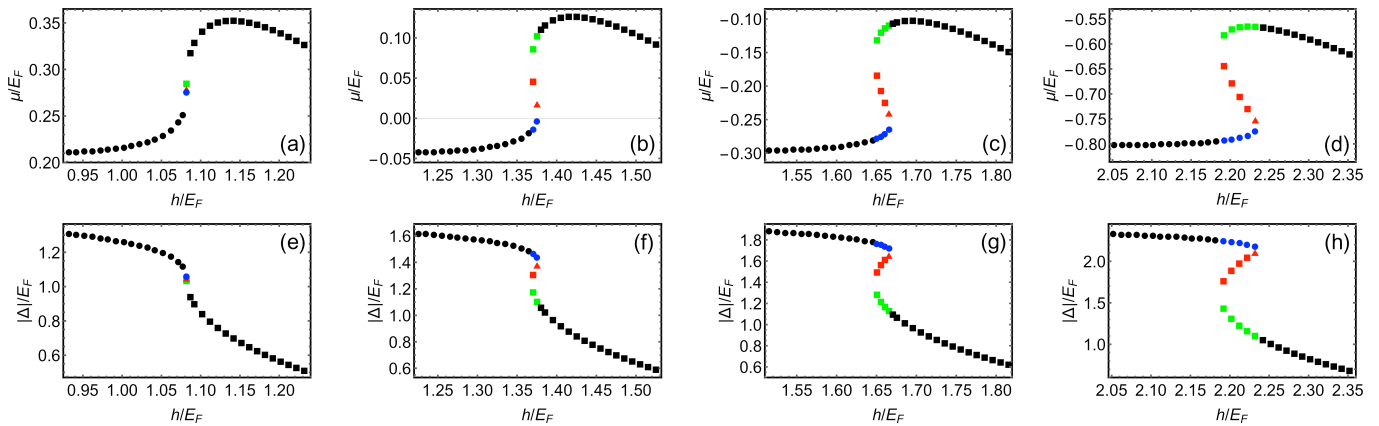


FIG. 6. Emergence of multiple pairs of self-consistent solutions for the chemical potential μ and s -wave pair-potential magnitude $|\Delta|$, indicated by colors. Results shown here are obtained for $\lambda k_F/E_F = 0.75$ (all panels) and $E_b/E_F = 1.001$ [panels (a) and (e)], 1.5 [panels (b) and (f)], 2.0 [panels (c) and (g)], 3.0 [panels (d) and (h)]. Circles (a triangle, squares) correspond to states where the system is nontopological (critical, topological).

for any value of h , $\mathcal{E}_{\text{gs}}^{(\text{MF})}$ has only a single minimum when plotted as a function of $|\Delta|$ for fixed μ , which occurs at a nonzero $|\Delta|$ and thus corresponds to a homogeneous superfluid ground state.

The search for solutions of the self-consistency conditions (7a) and (7b) for larger $E_b/E_F \lesssim 1$ continues to yield unique values of $|\Delta|$ and μ . See the examples shown in Fig. 4. However, an intricate complexity associated with self-consistent solutions starts to develop. As illustrated in Fig. 5, within an intermediate range of Zeeman energies, two additional extrema (specifically, a local minimum and a local maximum) start to appear in the $|\Delta|$ -dependence of the ground-state energy where μ has been fixed to its self-consistent value. Below the value $E_b^{(c)}$ associated with the critical end-point of the phase-separation region shown in Fig. 1, the unique solution of the self-consistency conditions still continues to be the global minimum of $\mathcal{E}_{\text{gs}}^{(\text{MF})}$, taken at the self-consistent μ , for any value of h . This is the case, e.g., for the system parameters used to calculate the results shown in Fig. 4(a,c). However, for $E_b \geq E_b^{(c)}$, which applies to Fig. 4(b,d), the self-consistently determined value for $|\Delta|$ ceases to be associated with the global minimum of $\mathcal{E}_{\text{gs}}^{(\text{MF})}$ at fixed self-consistent μ for Zeeman energies within a range $h_< < h < h_>$, corresponding instead to only a local minimum or even a maximum. This implies that no single-phase equilibrium ground state exists in the region $h_< < h < h_>$. Instead, phase separation into domains of different densities will occur if the system is driven into this regime. Even further in the BEC regime when $E_b > E_b^{(m)}$, multiple self-consistent pairs of values for $|\Delta|$ and μ emerge as illustrated in Fig. 6. Around each of these, additional zeros of the gap equation exist, as seen in Fig. 7. Now the range $h_< < h < h_>$ is defined to be the region where none of the self-consistent $|\Delta|$ values is associated with the global minimum of the ground-state energy $\mathcal{E}_{\text{gs}}^{(\text{MF})}$ when μ is corre-

sponding self-consistent value.

The appearance of multiple extrema in the $|\Delta|$ dependence of $\mathcal{E}_{\text{gs}}^{(\text{MF})}$ at fixed μ , leading to the self-consistent minimum ceasing to be the global minimum, indicates the presence of a first-order (noncontinuous) phase transition [29, 40]. A proper theoretical description of this situation requires the construction of various phase-coexistence scenarios [26, 27, 35], in analogy with treatments developed for the population-imbalanced Fermi gas without spin-orbit coupling [29, 42, 43, 48–52]. Here we defer the careful determination of the

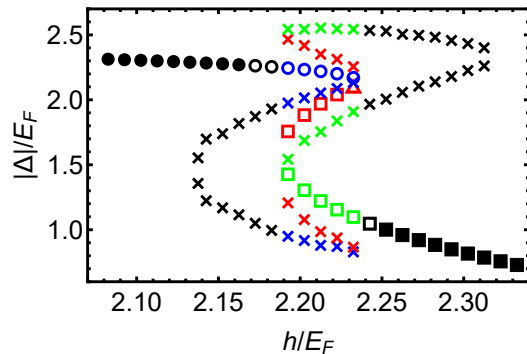


FIG. 7. Structure of multiple self-consistent and associated non-self-consistent solutions of the gap equation deep in the BEC limit. Results shown here are obtained for $\lambda k_F/E_F = 0.75$ and $E_b/E_F = 3.0$. Filled symbols indicate solutions of the self-consistency conditions that globally minimize the ground-state energy and thus correspond to proper equilibrium states of the system. Empty symbols (crosses) are associated with (non-)self-consistent values corresponding to a local minimum or maximum of the ground-state energy. Circles (a triangle, squares) indicate states where the system is nontopological (critical, topological). Multiple self-consistent solutions at a given h are distinguished by color. The same color is used to indicate their associated additional zeros in the gap equation.

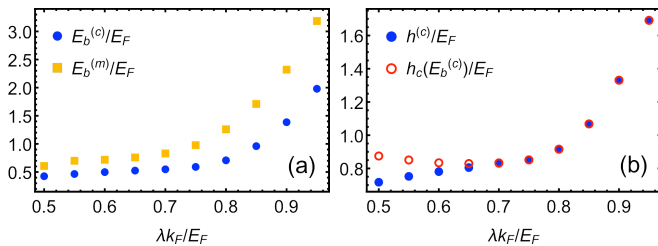


FIG. 8. Panel (a): Special values $E_b^{(c)}$ and $E_b^{(m)}$ for the two-particle bound-state energy E_b plotted as a function of the spin-orbit-coupling strength λ . Here $E_b^{(c)}$ is the value of E_b associated with the critical end point $(h^{(c)}, E_b^{(c)})$ of the phase-separation region in the E_b - h phase diagram. The value $E_b^{(m)}$ is the lower limit of bound-state energies for which multiple pairs of self-consistent solutions for μ and $|\Delta|$ exist. Panel (b): Dependence of $h^{(c)}$, the h coordinate of the critical end point of the phase-separation region in the E_b - h phase diagram, on the spin-orbit-coupling strength. For comparison, the critical field h_c [cf. Eq. (1)] at $E_b^{(c)}$ is also shown.

equilibrium ground state in the phase-separation region to future work [53]. Rather, we intend to discuss the properties of the adjacent uniform, single-phase regions for large E_b/E_F . To this end, we only need to map carefully the boundaries of the phase-separation region, i.e., the critical-Zeeman-energy curves $h_<$ and $h_>$. Results for representative values of the spin-orbit-coupling strength are given in Fig. 1. We find that the phase-separation region narrows as the spin-orbit-coupling parameter $\lambda k_F/E_F$ is increased, while simultaneously the critical end point $(h^{(c)}, E_b^{(c)})$ where the $h_<$ and $h_>$ curves merge shifts to larger coordinate values in the phase diagram. The full dependence of $E_b^{(c)}$ (and also of $E_b^{(m)}$) as a function of the dimensionless spin-orbit-coupling strength is plotted in Fig. 8(a), with the associated results for $h^{(c)}$ being provided in Fig. 8(b). Two different regimes, corresponding to small and large values of $\lambda k_F/E_F$, can be identified, where the former (latter) is characterized by the $h^{(c)}$ values diverging from (coinciding with) the critical field h_c for $E_b = E_b^{(c)}$.

The curves for $h_<(E_b)$ and $h_>(E_b)$ in the phase diagram delimit the phase-separation region associated with a first-order transition between different superfluid states. In those parts of the phase diagram outside this region where only a single pair of self-consistent values for μ and $|\Delta|$ exists, a curve $h_c(E_b)$ can be defined via Eq. (1) that separates the part of the phase diagram where the system is an ordinary nontopological superfluid (NSF, for $h < h_c$) from the part where the ground state corresponds to a topological superfluid (TSF, for $h > h_c$). In particular, for $E_b < E_b^{(c)}$, only this second-order topological transition occurs. However, beyond the point where the curve for $h_c(E_b)$ crosses that of $h_>(E_b)$, solutions of the self-consistency conditions that are critical, i.e., satisfy $h = \sqrt{\mu^2 + |\Delta|^2}$, continue to exist but are no longer a global minimum of

the ground-state energy at fixed μ . At the same time, the homogeneous-superfluid states existing for $h > h_>$ satisfy $h > \sqrt{\mu^2 + |\Delta|^2}$ and are thus in the topological regime. Hence, beyond the crossing point of $h_c(E_b)$ and $h_>(E_b)$, the topological transition is of first order. The phase boundary of the homogeneous 2D TSF is therefore delineated by $h_{\max}(E_b) = \max\{h_c(E_b), h_>(E_b)\}$. Due to the tendency of $|\Delta|$ to monotonically decrease with h in regions where a self-consistent solution is associated with the system's equilibrium ground state (see Figs. 3, 5, and 7), h_{\max} is also the Zeeman energy for which $|\Delta|$ is maximized in the TSF phase at fixed E_b . We now focus on the properties of the single-phase ground states adjacent to the phase-separation region at large $E_b > E_b^{(c)}$.

The typical phenomenology of the BCS-to-BEC crossover for s -wave pairing entails a shift of the dispersion minimum to $k = 0$, Bogoliubov quasi-particles becoming mostly particle-like, and the momentum-space density distribution losing its typical Fermi-surface-like shape [30–34]. This exact scenario is played out for our more complicated system of interest in the NSF phase. See Fig. 9. In contrast, as illustrated by Fig. 10, all features associated with effective chiral p -wave pairing in the spin- \uparrow channel remain present throughout the BCS-to-BEC crossover in the TSF phase. In particular, the momentum-space density distribution shows a distinctive

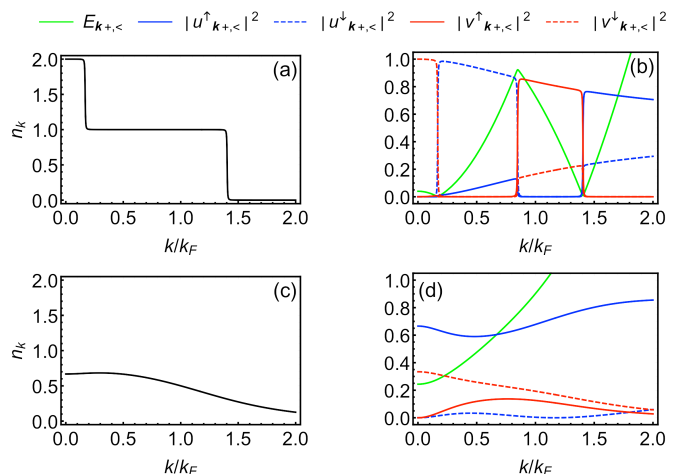


FIG. 9. Expected BCS and BEC characteristics are exhibited in the nontopological-superfluid (NSF) phase of a spin-orbit-coupled 2D Fermi gas. The situation depicted here corresponds to $\lambda k_F/E_F = 0.75$. Panels (a) and (b) [(c) and (d)] show results for $E_b/E_F = 0.010$ [3.0] and $h = h_c - 0.04 E_F$ [$h_<$, corresponding to the filled circle with maximum h in Fig. 7]. The presence (absence) of Fermi-surface features in the momentum-space density distribution n_k is typical for the BCS (BEC) limit of s -wave pairing. Also the shift of the excitation gaps in the quasiparticle dispersion (the lowest positive-energy branch $E_{k+,<}$ is shown as the green curve) from finite k to $k = 0$ is a prominent characteristic of the BEC limit, as is the suppression of all but one Bogoliubov amplitude (the one corresponding to spin- \uparrow Nambu particles, indicated by the solid blue curve).

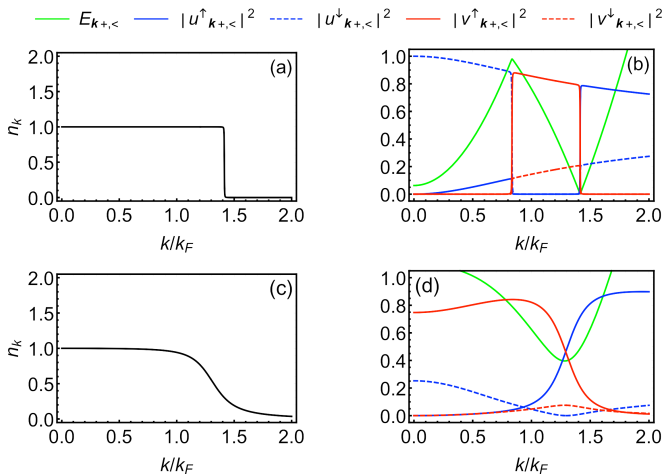


FIG. 10. Persistence of a Fermi surface, and all other canonical features associated with chiral p -wave pairing, in the topological-superfluid (TSF) phase of a spin-orbit-coupled 2D Fermi gas throughout the BCS-to-BEC crossover of the underlying s -wave pairing. Results shown are for $\lambda k_F/E_F = 0.75$, with panels (a) and (b) [(c) and (d)] pertaining to $E_b/E_F = 0.010$ [3.0] and $h = h_c + 0.04 E_F$ [$h_{>}$], corresponding to the filled square with minimum h in Fig. 7]. Solid (dashed) blue and red curves show the spin- \uparrow (\downarrow)-particle and spin- \uparrow (\downarrow)-hole probability densities, respectively, for the lowest positive-energy branch of Bogoliubov-quasiparticle excitations whose energy dispersion is shown as the green curve. A significant distinction of the BEC limit is a purer chiral- p -wave character of the low-energy degrees of freedom, as signified by a larger gap in the quasiparticle dispersion and clearer dominance of the spin- \uparrow Nambu-spinor amplitudes.

Fermi-surface feature even deep in the BEC regime for s -wave pairing, which is unexpected for situations where the chemical potential is negative [54]. As can be seen in Fig. 10, the most visible attributes that distinguish the TSF in the BEC limit from that arising in the BCS limit are the increased magnitude of the low-energy excitation gap Δ_{pw} and the strong suppression of the minority-spin degrees of freedom. The clear dominance of the spin- \uparrow Bogoliubov amplitudes representing chiral p -wave pairing is one of the favorable qualities exhibited by the TSF realized in the BEC limit. In addition, a larger magnitude of Δ_{pw} should help to reduce the influence of many experimental nonidealities, including thermal fluctuations. Thus, the TSF realized in the BEC limit of the underlying s -wave pairing constitutes both a purer and a more-robust version of the highly sought-after chiral p -wave order.

IV. CONCLUSIONS AND OUTLOOK

We have investigated the strongly interacting limit of the 2D Fermi gas with s -wave pairing, with fixed particle

density and subject to both spin-orbit coupling and Zeeman spin splitting. Characteristic features of the phase diagram as a function of two-particle binding energy E_b and Zeeman energy h are elucidated and the properties of the homogeneous superfluid phases studied in greater detail. In particular, we tracked the boundaries of the homogeneous nontopological and topological superfluids. The second-order topological-transition line $h_c(E_b)$, with h_c defined via Eq. (1), is truncated by a phase-separation region that emerges for E_b larger than a critical value $E_b^{(c)}$ that depends on the spin-orbit-coupling strength (cf. Figs. 1 and 8). As a result, the topological transition is of first order in the limit of large E_b/E_F .

The homogeneous nontopological phase exhibits all of the expected features commonly associated with the BCS-to-BEC crossover for s -wave pairing, especially the shrinking, and eventual disappearance, of an underlying Fermi surface as the Cooper-pair binding energy is increased. See Fig. 9(c,d). In contrast, as illustrated in Fig. 10, the topological superfluid phase always retains the basic properties of the BCS regime, including the Fermi-surface characteristics, even in the limit of large E_b/E_F . This effect demonstrates the continuity of topological protection through the BCS-to-BEC crossover.

Physical realizations of the model system considered in the present work are currently available, e.g., in ultra-cold-atom gases [55] and solid-state heterostructures [56, 57]. State-of-the-art experimental techniques [58] could be utilized, or related theoretical proposals [59] may be pursued, to confirm the re-appearance of a Fermi surface as the Zeeman energy is tuned across the topological transition when the system is in the BEC limit of the underlying s -wave pairing. Compared to the BCS limit, chiral p -wave superfluidity realized in the BEC limit has a larger excitation gap and is less obscured by minority-spin degrees of freedom, making it the ideal platform for exploring exotic Majorana excitations in vortices [12–14] and their potential use for topological quantum-information-processing paradigms [15]. Future work could focus on elucidating also the evolution and properties of topological superfluids within the phase-separation region.

ACKNOWLEDGMENTS

The authors gratefully acknowledge useful discussions with W. Belzig, C. Bruder, M. M. Parish, D. M. Stamper-Kurn, and O. P. Sushkov. This work was partially supported by the Marsden Fund of New Zealand (contract no. MAU1604), from government funding managed by the Royal Society Te Apārangi.

- [1] Masatoshi Sato and Yoichi Ando, “Topological superconductors: a review,” *Rep. Prog. Phys.* **80**, 076501 (2017).
- [2] Liang Fu and C. L. Kane, “Superconducting proximity effect and Majorana fermions at the surface of a topological insulator,” *Phys. Rev. Lett.* **100**, 096407 (2008).
- [3] Chuanwei Zhang, Sumanta Tewari, Roman M. Lutchyn, and S. Das Sarma, “ $p_x + ip_y$ superfluid from s-wave interactions of fermionic cold atoms,” *Phys. Rev. Lett.* **101**, 160401 (2008).
- [4] Jay D. Sau, Roman M. Lutchyn, Sumanta Tewari, and S. Das Sarma, “Generic new platform for topological quantum computation using semiconductor heterostructures,” *Phys. Rev. Lett.* **104**, 040502 (2010).
- [5] Jason Alicea, “Majorana fermions in a tunable semiconductor device,” *Phys. Rev. B* **81**, 125318 (2010).
- [6] Masatoshi Sato, Yoshiro Takahashi, and Satoshi Fujimoto, “Non-abelian topological orders and Majorana fermions in spin-singlet superconductors,” *Phys. Rev. B* **82**, 134521 (2010).
- [7] J. Brand, L. A. Toikka, and U. Zülicke, “Accurate projective two-band description of topological superfluidity in spin-orbit-coupled Fermi gases,” *SciPost Phys.* **5**, 16 (2018).
- [8] Catherine Kallin and John Berlinsky, “Chiral superconductors,” *Rep. Prog. Phys.* **79**, 054502 (2016).
- [9] R. Jackiw and C. Rebbi, “Solitons with fermion number $\frac{1}{2}$,” *Phys. Rev. D* **13**, 3398–3409 (1976).
- [10] N. B. Kopnin and M. M. Salomaa, “Mutual friction in superfluid ^3He : Effects of bound states in the vortex core,” *Phys. Rev. B* **44**, 9667–9677 (1991).
- [11] G. E. Volovik, “Fermion zero modes on vortices in chiral superconductors,” *JETP Lett.* **70**, 609–614 (1999).
- [12] N. Read and Dmitry Green, “Paired states of fermions in two dimensions with breaking of parity and time-reversal symmetries and the fractional quantum Hall effect,” *Phys. Rev. B* **61**, 10267–10297 (2000).
- [13] D. A. Ivanov, “Non-Abelian statistics of half-quantum vortices in p -wave superconductors,” *Phys. Rev. Lett.* **86**, 268–271 (2001).
- [14] V. Gurarie and L. Radzihovsky, “Zero modes of two-dimensional chiral p -wave superconductors,” *Phys. Rev. B* **75**, 212509 (2007).
- [15] Sankar Das Sarma, Michael Freedman, and Chetan Nayak, “Majorana zero modes and topological quantum computation,” *npj Quant. Inf.* **1**, 15001 (2015).
- [16] Florian Loder, Arno P Kampf, and Thilo Kopp, “Route to topological superconductivity via magnetic field rotation,” *Sci. Rep.* **5**, 15302 (2015).
- [17] Roland Winkler, *Spin-Orbit Coupling Effects in Two-Dimensional Electron and Hole Systems* (Springer, Berlin, 2003).
- [18] Hui Zhai, “Degenerate quantum gases with spin-orbit coupling: a review,” *Rep. Prog. Phys.* **78**, 026001 (2015).
- [19] Wei Zhang, Wei Yi, and Carlos A. R. Sá de Melo, eds., *Synthetic Spin-Orbit Coupling in Cold Atoms* (World Scientific, Singapore, 2018).
- [20] A. J. Leggett, “Diatomic molecules and Cooper pairs,” in *Modern Trends in the Theory of Condensed Matter*, edited by Andrzej Pękalski and Jerzy A. Przystawa (Springer, Berlin, 1980) pp. 13–27.
- [21] A. J. Leggett, “Cooper pairing in spin-polarized Fermi systems,” *J. Phys. Colloques* **41**(C7), 19–26 (1980).
- [22] Mohit Randeria, Ji-Min Duan, and Lih-Yir Shieh, “Superconductivity in a two-dimensional Fermi gas: Evolution from Cooper pairing to Bose condensation,” *Phys. Rev. B* **41**, 327–343 (1990).
- [23] Meera M. Parish, “The BCS–BEC crossover,” in *Quantum Gas Experiments*, edited by P. Törmä and K. Sengstock (Imperial College Press, London, 2015) pp. 179–197.
- [24] Giancarlo Calvanese Strinati, Pierbiagio Pieri, Gerd Röpke, Peter Schuck, and Michael Urban, “The BCS–BEC crossover: From ultra-cold Fermi gases to nuclear systems,” *Phys. Repts.* **738**, 1–76 (2018).
- [25] The mean-field approximation generally yields useful insight into zero-temperature phases, even when interactions are strong [43, 60]. Quantitatively more accurate predictions, in particular for finite temperature, require more sophisticated approaches [61–64].
- [26] W. Yi and G.-C. Guo, “Phase separation in a polarized Fermi gas with spin-orbit coupling,” *Phys. Rev. A* **84**, 031608 (2011).
- [27] Xiaosen Yang and Shaolong Wan, “Phase diagram of a uniform two-dimensional Fermi gas with spin-orbit coupling,” *Phys. Rev. A* **85**, 023633 (2012).
- [28] See, e.g., Fig. 2(a) in Ref. [29].
- [29] Lianyi He and Pengfei Zhuang, “Phase diagram of a cold polarized Fermi gas in two dimensions,” *Phys. Rev. A* **78**, 033613 (2008).
- [30] Rajdeep Sensarma, Mohit Randeria, and Nandini Trivedi, “Can one determine the underlying Fermi surface in the superconducting state of strongly correlated systems?” *Phys. Rev. Lett.* **98**, 027004 (2007).
- [31] P. Nozières and S. Schmitt-Rink, “Bose condensation in an attractive fermion gas: From weak to strong coupling superconductivity,” *J. Low Temp. Phys.* **59**, 195–211 (1985).
- [32] Qijin Chen, Jelena Stajic, Shina Tan, and K. Levin, “BCS–BEC crossover: From high temperature superconductors to ultracold superfluids,” *Phys. Rep.* **412**, 1–88 (2005).
- [33] G. E. Astrakharchik, J. Boronat, J. Casulleras, and S. Giorgini, “Momentum distribution and condensate fraction of a fermion gas in the BCS-BEC crossover,” *Phys. Rev. Lett.* **95**, 230405 (2005).
- [34] Hao Shi, Peter Rosenberg, Simone Chiesa, and Shiwei Zhang, “Rashba spin-orbit coupling, strong interactions, and the BCS-BEC crossover in the ground state of the two-dimensional Fermi gas,” *Phys. Rev. Lett.* **117**, 040401 (2016).
- [35] Kangjun Seo, Li Han, and C. A. R. Sá de Melo, “Topological phase transitions in ultracold Fermi superfluids: The evolution from Bardeen-Cooper-Schrieffer to Bose-Einstein-condensate superfluids under artificial spin-orbit fields,” *Phys. Rev. A* **85**, 033601 (2012).
- [36] Lianyi He and Xu-Guang Huang, “Superfluidity and collective modes in Rashba spin-orbit coupled Fermi gases,” *Ann. Phys. (Leipzig)* **337**, 163–207 (2013).
- [37] P. G. de Gennes, *Superconductivity of Metals and Alloys* (Addison-Wesley, Reading, MA, 1989).
- [38] Our notation adheres to that used in Ref. [7].
- [39] We focus here only on types of spin-orbit coupling that

- depend linearly on the components of \mathbf{k} . Typical examples are the Dirac, 2D-Rashba, and 2D-Dresselhaus functional forms corresponding to $\lambda_{\mathbf{k}} = \lambda(k_x - ik_y)$, $\lambda i(k_x - ik_y)$, and $\lambda(k_x + ik_y)$, respectively.
- [40] Jing Zhou, Wei Zhang, and Wei Yi, “Topological superfluid in a trapped two-dimensional polarized Fermi gas with spin-orbit coupling,” *Phys. Rev. A* **84**, 063603 (2011).
- [41] Leo Radzihovsky and Daniel E. Sheehy, “Imbalanced Feshbach-resonant Fermi gases,” *Rep. Prog. Phys.* **73**, 076501 (2010).
- [42] Daniel E. Sheehy and Leo Radzihovsky, “BEC–BCS crossover, phase transitions and phase separation in polarized resonantly-paired superfluids,” *Ann. Phys. (NY)* **322**, 1790–1924 (2007).
- [43] M. M. Parish, F. M. Marchetti, A. Lamacraft, and B. D. Simons, “Finite-temperature phase diagram of a polarized Fermi condensate,” *Nat. Phys.* **3**, 124–128 (2007).
- [44] Daniel E. Sheehy and Leo Radzihovsky, “Comment on ‘Superfluid stability in the BEC-BCS crossover’,” *Phys. Rev. B* **75**, 136501 (2007).
- [45] G. Sarma, “On the influence of a uniform exchange field acting on the spins of the conduction electrons in a superconductor,” *J. Phys. Chem. Solids* **24**, 1029–1032 (1963).
- [46] A. Lamacraft and F. M. Marchetti, “Spinodal decomposition in polarized Fermi superfluids,” *Phys. Rev. B* **77**, 014511 (2008).
- [47] Lianyi He and Pengfei Zhuang, “Stable Sarma state in two-band Fermi systems,” *Phys. Rev. B* **79**, 024511 (2009).
- [48] Paulo F. Bedaque, Heron Caldas, and Gautam Rupak, “Phase separation in asymmetrical fermion superfluids,” *Phys. Rev. Lett.* **91**, 247002 (2003).
- [49] J. Carlson and Sanjay Reddy, “Asymmetric two-component fermion systems in strong coupling,” *Phys. Rev. Lett.* **95**, 060401 (2005).
- [50] Daniel E. Sheehy and Leo Radzihovsky, “BEC-BCS crossover in ‘magnetized’ Feshbach-resonantly paired superfluids,” *Phys. Rev. Lett.* **96**, 060401 (2006).
- [51] D. T. Son and M. A. Stephanov, “Phase diagram of a cold polarized Fermi gas,” *Phys. Rev. A* **74**, 013614 (2006).
- [52] Jia-Jia Du, Cheng Chen, and Jun-Jun Liang, “Asymmetric two-component Fermi gas in two dimensions,” *Phys. Rev. A* **80**, 023601 (2009).
- [53] This task becomes particularly challenging for the part of the phase diagram where multiple self-consistent solutions of the gap equation exist at fixed h . Generally, two of these correspond to minima of the ground-state energy taken at fixed μ , and their combined evolution between global- or local-minimum status needs to be tracked.
- [54] See, e.g., Ref. [32]. Similar behavior to the one found by us here for the 2D TSF seems to also be implicit in results that were presented for the 3D spin-orbit-coupled Fermi superfluid (see, e.g., Fig. 6 in Ref. [35]) but whose physical significance was not discussed.
- [55] Zengming Meng, Lianghui Huang, Peng Peng, Donghao Li, Liangchao Chen, Yong Xu, Chuanwei Zhang, Pengjun Wang, and Jing Zhang, “Experimental observation of a topological band gap opening in ultracold Fermi gases with two-dimensional spin-orbit coupling,” *Phys. Rev. Lett.* **117**, 235304 (2016).
- [56] M. Ben Shalom, M. Sachs, D. Rakhmilevitch, A. Palevski, and Y. Dagan, “Tuning spin-orbit coupling and superconductivity at the SrTiO₃/LaAlO₃ interface: A magnetotransport study,” *Phys. Rev. Lett.* **104**, 126802 (2010).
- [57] J. Shabani, M. Kjaergaard, H. J. Suominen, Younghyun Kim, F. Nichele, K. Pakrouski, T. Stankevic, R. M. Lutchyn, P. Krogstrup, R. Feidenhans’l, S. Kraemer, C. Nayak, M. Troyer, C. M. Marcus, and C. J. Palmstrøm, “Two-dimensional epitaxial superconductor-semiconductor heterostructures: A platform for topological superconducting networks,” *Phys. Rev. B* **93**, 155402 (2016).
- [58] C. A. Regal, M. Greiner, S. Giorgini, M. Holland, and D. S. Jin, “Momentum distribution of a Fermi gas of atoms in the BCS-BEC crossover,” *Phys. Rev. Lett.* **95**, 250404 (2005).
- [59] W. Yi and L.-M. Duan, “Detecting the breached-pair phase in a polarized ultracold Fermi gas,” *Phys. Rev. Lett.* **97**, 120401 (2006).
- [60] Andrea M. Fischer and Meera M. Parish, “BCS-BEC crossover in a quasi-two-dimensional Fermi gas,” *Phys. Rev. A* **88**, 023612 (2013).
- [61] M. Yu. Kuchiev and O. P. Sushkov, “Many-body correlation corrections to superconducting pairing in two dimensions,” *Phys. Rev. B* **53**, 443–448 (1996).
- [62] W. Yi and L.-M. Duan, “Phase diagram of a polarized Fermi gas across a Feshbach resonance in a potential trap,” *Phys. Rev. A* **74**, 013610 (2006).
- [63] G. Bertaina and S. Giorgini, “BCS-BEC crossover in a two-dimensional Fermi gas,” *Phys. Rev. Lett.* **106**, 110403 (2011).
- [64] Lianyi He, Haifeng Lü, Gaoqing Cao, Hui Hu, and Xia-Ji Liu, “Quantum fluctuations in the BCS-BEC crossover of two-dimensional Fermi gases,” *Phys. Rev. A* **92**, 023620 (2015).